Nonequilibrium dynamical mean field theory

International summer school on Computational Quantum Materials 2018

Jouvence, Canada (June 2018)

Philipp Werner

Department of Physics, University of Fribourg, 1700 Fribourg, Switzerland

I. INTRODUCTION

The low-energy properties of correlated materials are often characterized by competing interactions, which lead to rich phase diagrams and large responses to changes in pressure, doping or external fields. Many of these effects cannot be explained by perturbative approaches, and a direct numerical simulation of the relevant lattice models is often not possible, which makes a theoretical understanding very challenging. A relatively recent experimental trend is to explore the *nonequilibrium* properties of such materials. By driving the system out of equilibrium, one can hope to disentangle competing effects with different intrinsic time-scales, and thus shed new light on complicated, intertwined correlation phenomena.[1] An even more exciting prospect is the possibility to "tune" material properties by external driving,[2] or the discovery of "hidden states" of correlated materials, which cannot be accessed via thermal pathways.[3]

Stimulated by these experimental developments, a growing theoretical effort is focusing on the simulation of the nonequilibrium dynamics in correlated lattice systems. Here, we discuss one of the most promising approaches – the nonequilibrium generalization of dynamical mean field theory (DMFT).[4,5] This method, which is formulated in the thermodynamic limit, simplifies the computational task by mapping the lattice problem to a self-consistent solution of a quantum impurity model. If a suitable "impurity solver" is used, it can treat local interactions of arbitrary strength, highly excited states, as well as the eventual thermalization of the system after a perturbation. We will start by explaining the main ideas and approximations behind the well-established equilibrium DMFT formalism,[6] and then show how it can be extended to situations in which an equilibrium system at time $t = 0$ is perturbed either by a time-dependent change in an interaction parameter, or by a time-

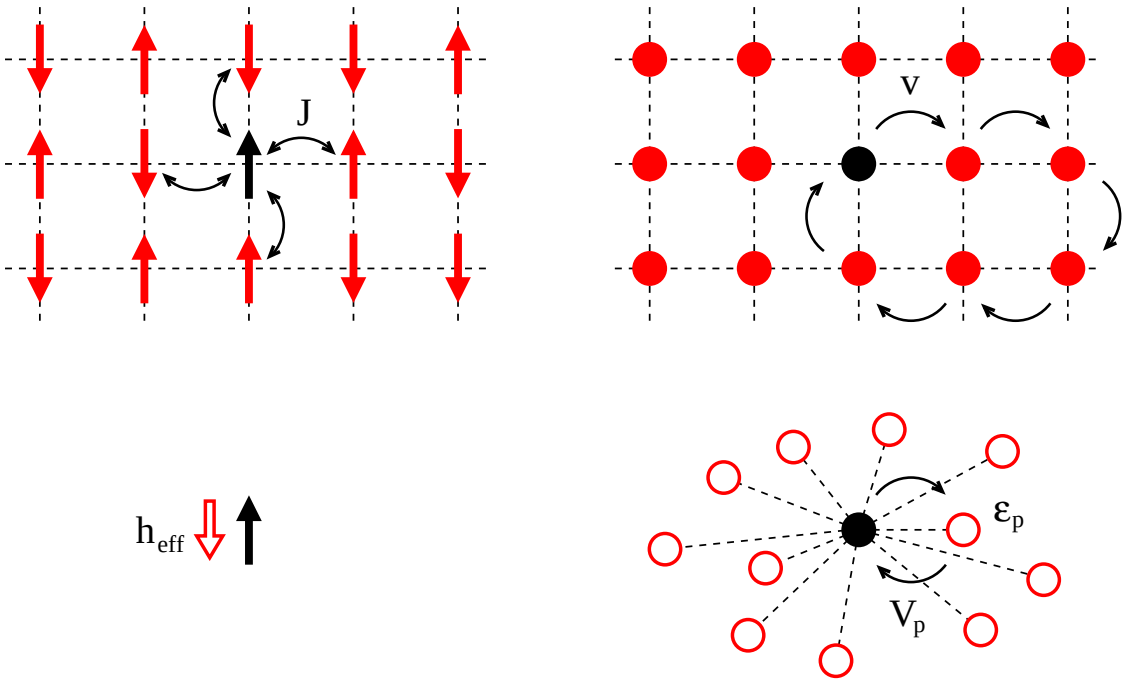

FIG. 1: Left panels: Mapping of the classical Ising model to an effective single-site model (spin in an external magnetic field). Right panels: Mapping of the Hubbard model to an effective single-site model (one correlated site in an uncorrelated bath).

dependent electric field. We illustrate the nonequilibrium DMFT method with two results for the one-band Hubbard model: (i) the dynamical band narrowing or band inversion induced by periodic electric fields, and (ii) the influence of nonthermal fixed points on the relaxation dynamics in quenched antiferromagnets.

II. DYNAMICAL MEAN-FIELD THEORY

A. Single-site effective model

To motivate the basic strategy behind the DMFT approach, and to appreciate the nature of the approximation, we first recall the static mean-field theory for the classical Ising model, illustrated in the left-hand panels of Fig. 1. There, we have a lattice of interacting Ising spins with interaction J between nearest-neighbor spins. In the mean-field approximation, we focus on one particular spin, s_0, and replace the remaining degrees of freedom by an effective external magnetic field $h_{\rm eff} = zmJ$, where z is the coordination number and m is

the magnetization per site. The lattice model

$$H^{\text{Ising}} = -J \sum_{\langle ij \rangle} s_i s_j \tag{1}$$

thus maps to the single-site effective model

$$H^{\text{Ising}}_{\text{eff}} = -h_{\text{eff}} s_0. \tag{2}$$

For this model, the magnetization at inverse temperature $\beta = 1/T$ is

$$m_{\text{eff}} = \tanh(\beta h_{\text{eff}}). \tag{3}$$

If we identify the magnetization m of the lattice model with the magnetization m_{eff} of the single-site effective model, we obtain the self-consistency condition

$$m \equiv m_{\text{eff}} = \tanh(\beta z J m), \tag{4}$$

which implicitly determines the *mean field* h_{eff}. One can find the self-consistent solution by iteration.

We now turn to the generic model for correlated electron materials, the Hubbard model, and apply the same strategy.[6] For simplicity, we consider a one-band Hubbard model

$$H_{\text{Hubbard}} = -v \sum_{\langle ij \rangle \sigma} (d^\dagger_{i\sigma} d_{j\sigma} + d^\dagger_{j\sigma} d_{i\sigma}) + U \sum_i n_{i\uparrow} n_{i\downarrow} - \mu \sum_{i\sigma} n_{i\sigma}, \tag{5}$$

which describes electrons hopping between nearest neighbor sites of some lattice with amplitude v. Two electrons on the same site interact with a repulsive energy U. We added a chemical potential term because we will work in the grand canonical ensemble. The noninteracting dispersion ϵ_k is obtained as the Fourier transform of the the hopping matrix. For example, in the case of a one-dimensional lattice with lattice spacing a, $\epsilon_k = -2v\cos(ka)$.

Inspired by the Weiss molecular-field strategy, we focus on one particular site of the lattice (black dot in the right hand panels of Fig. 1) and replace the remaining degrees of freedom of the model by a bath of non-interacting levels and a hybridization term that connects the interacting site to the bath. The effective single-site problem thus becomes an *Anderson impurity model*,

$$H_{\text{imp}} = \sum_{p\sigma} \varepsilon_p c^\dagger_{p\sigma} c_{p\sigma} + \sum_{p\sigma} (V_{p\sigma} d^\dagger_\sigma c_{p\sigma} + V^*_{p\sigma} c^\dagger_{p\sigma} d_\sigma) + U n_\uparrow n_\downarrow - \mu(n_\uparrow + n_\downarrow). \tag{6}$$

Here, the $d^\dagger$ create electrons on the impurity (black dot), $n_\sigma = d^\dagger_\sigma d_\sigma$, and the $c^\dagger_p$ create electrons in bath states (empty dots) labeled by a quantum number p. In this effective single-site model, hoppings from the impurity into the bath and back (bottom right panel of Fig. 1) represent processes in the original model where an electron hops from the black site into the lattice and returns to it after some excursion through the lattice (top right panel of Fig. 1). The hybridization parameters V_p give the amplitudes for such transitions.

Our task now is to optimize the parameters ε_p and V_p such that the bath of the Anderson impurity model mimics the lattice environment as closely as possible. These parameters are the analogues of $h_{\rm eff}$ and thus need to be adjusted self-consistently. The self-consistent solution is constructed in such a way that the impurity Green's function $G_{\rm imp}(i\omega_n)$ reproduces the *local* lattice Green's function $G_{\rm loc}(i\omega_n) \equiv G_{i,i}(i\omega_n)$. In other words, if $G(k, i\omega_n)$ is the momentum-dependent lattice Green's function of the Hubbard model, we seek bath parameters and hybridizations such that

$$\int (dk) G(k, i\omega_n) \equiv G_{\rm imp}(i\omega_n), \tag{7}$$

where $\int (dk)$ denotes a normalized integral over the Brillouin zone. This self-consistency equation is the analogue of (4).

B. Impurity action

It is often convenient to integrate out the noninteracting bath degrees of freedom and to express the partition function of the Anderson impurity model as

$$Z_{\rm imp} = {\rm Tr}_d\big[\mathcal{T} e^{-S_{\rm imp}}\big], \tag{8}$$

with the action $S_{\rm imp} = S_{\rm loc} + S_{\rm hyb}$ given by

$$S_{\rm loc} = \int_0^\beta d\tau \Big[U n_\uparrow(\tau) n_\downarrow(\tau) - \mu(n_\uparrow(\tau) + n_\downarrow(\tau))\Big], \tag{9}$$

$$S_{\rm hyb} = \sum_\sigma \int_0^\beta d\tau d\tau' d^\dagger_\sigma(\tau') \Delta_\sigma(\tau' - \tau) d_\sigma(\tau), \tag{10}$$

and $\mathcal{T}$ the time-ordering operator. The impurity Green's function becomes

$$G_{\rm imp}(\tau) = -\langle \mathcal{T} d(\tau) d^\dagger(0)\rangle_{S_{\rm imp}} = -\frac{1}{Z_{\rm imp}} {\rm Tr}_d\big[\mathcal{T} e^{-S_{\rm imp}} d(\tau) d^\dagger(0)\big]. \tag{11}$$

The hybridization function $\Delta_\sigma(\tau' - \tau)$ in Eq. (10) represents the amplitude for hopping from the impurity into the bath at time τ and back onto the impurity at time τ'. It is a function of the bath energies and hybridization amplitudes and is most conveniently expressed in Matsubara frequency space [$\Delta(i\omega_n) = \int_0^\beta d\tau\, e^{i\omega_n\tau}\Delta(\tau)\,, \Delta(\tau) = \frac{1}{\beta}\sum_n e^{-i\omega_n\tau}\Delta(i\omega_n)$]:

$$\Delta_\sigma(i\omega_n) = \sum_p \frac{|V_{p\sigma}|^2}{i\omega_n - \varepsilon_p}. \tag{12}$$

It is also useful to introduce the Green's function of the non-interacting impurity ("Weiss Green's function"), $\mathcal{G}_0$, which is related to the hybridization function by

$$[\mathcal{G}_{0\sigma}]^{-1}(i\omega_n) = i\omega_n + \mu - \Delta_\sigma(i\omega_n). \tag{13}$$

$\Delta(\tau)$ [or equivalently $\mathcal{G}_0(\tau)$] contains all the relevant information about the bath and thus plays the role of the mean field. It is a *dynamical* mean field, because the hybridization function [or Weiss Green's function] depends on time or frequency.

C. DMFT approximation

We obtain the solution of Eq. (7) iteratively. However, in contrast to the Ising case (4), it is not immediately clear how we can use this self-consistency condition to update the dynamical mean field. To define a practical procedure, we have to relate the left-hand-side of Eq. (7) to impurity model quantities. This step involves, as the essential approximation of the DMFT method, a significant simplification of the momentum-dependence of the lattice self-energy.

The self-energy describes the effect of interactions on the propagation of electrons. In the non-interacting model, the lattice Green's function is $G_0(k, i\omega_n) = [i\omega_n + \mu - \epsilon_k]^{-1}$, with ϵ_k the Fourier transform of the hopping matrix. The Green's function of the interacting model is $G(k, i\omega_n) = [i\omega_n + \mu - \epsilon_k - \Sigma(k, i\omega_n)]^{-1}$ with $\Sigma(k, i\omega_n)$ the lattice self-energy. Therefore

$$\Sigma(k, i\omega_n) = G_0^{-1}(k, i\omega_n) - G^{-1}(k, i\omega_n). \tag{14}$$

Similarly, we obtain the impurity self-energy as

$$\Sigma_{\rm imp}(i\omega_n) = \mathcal{G}_0^{-1}(i\omega_n) - G_{\rm imp}^{-1}(i\omega_n), \tag{15}$$

with $\mathcal{G}_0^{-1}$ defined in Eq. (13). The DMFT approximation is the identification of the lattice self-energy with the momentum-independent impurity self-energy,

$$\Sigma(k, i\omega_n) \approx \Sigma_{\rm imp}(i\omega_n). \tag{16}$$

This approximation enables us to rewrite the self-consistency equation (7) as

$$\int (dk)[i\omega_n + \mu - \epsilon_k - \Sigma_{\rm imp}(i\omega_n)]^{-1} \equiv G_{\rm imp}(i\omega_n). \tag{17}$$

Since both $G_{\rm imp}(i\omega_n)$ and $\Sigma_{\rm imp}(i\omega_n)$ are determined by the impurity model parameters ε_p and V_p (or the function $\Delta(\tau)$ or $\mathcal{G}_0(\tau)$), Eq. (17) defines a self-consistency condition for these parameters (or functions).

D. DMFT self-consistency loop

We now formulate the self-consistency loop for the Weiss Green's function $\mathcal{G}_0(i\omega_n)$. Starting from an arbitrary initial $\mathcal{G}_0(i\omega_n)$ (for example, the local Green's function of the noninteracting lattice model), we iterate the following steps until convergence:

1. Solve the impurity problem, that is, compute the impurity Green's function $G_{\rm imp}(i\omega_n)$ for the given $\mathcal{G}_0(i\omega_n)$,

2. Extract the self-energy of the impurity model: $\Sigma_{\rm imp}(i\omega_n) = \mathcal{G}_0^{-1}(i\omega_n) - G_{\rm imp}^{-1}(i\omega_n)$,

3. Identify the lattice self-energy with the impurity self-energy, $\Sigma(k, i\omega_n) = \Sigma_{\rm imp}(i\omega_n)$ (DMFT approximation), and compute the local lattice Green's function $G_{\rm loc}(i\omega_n) = \int (dk)[i\omega_n + \mu - \epsilon_k - \Sigma_{\rm imp}(i\omega_n)]^{-1}$,

4. Apply the DMFT self-consistency condition, $G_{\rm loc}(i\omega_n) = G_{\rm imp}(i\omega_n)$, and use it to define a new Weiss Green's function $\mathcal{G}_0^{-1}(i\omega_n) = G_{\rm loc}^{-1}(i\omega_n) + \Sigma_{\rm imp}(i\omega_n)$.

The computationally expensive step is the solution of the impurity problem (Step 1). When the loop converges, the bath contains information about the topology of the lattice (through the density of states), and about the phase (metal, Mott insulator, antiferromagnetic insulator, ...). The impurity, which exchanges electrons with the bath, thus feels, at least to some extent, as if it were a site of the lattice.

Obviously, a single-site impurity model does not capture all the physics. In particular, the DMFT approximation neglects all spatial fluctuations. These fluctuations are important, for example, in low-dimensional systems. The DMFT formalism is believed to provide a qualitatively correct description of three-dimensional unfrustrated lattice models. It becomes exact in the limit of infinite dimension[7] or infinite coordination number (where spatial fluctuations are negligible), in the non-interacting limit ($U = 0$ implies $\Sigma = 0$), and in the atomic limit ($t = 0$ implies $\Delta = 0$).

E. Cluster extensions

To capture the effect of short-range spatial fluctuations, cluster extensions of dynamical mean field theory were developed.[8] In these extensions, a cluster of several sites, instead of a single site, is embedded in a self-consistently determined bath. This embedding allows to describe the short-range spatial correlations on the cluster explicitly, while treating the longer range correlations on a mean-field level.

In a cluster DMFT, we divide the lattice into a superlattice of clusters containing n_c sites and apply the DMFT procedure to the superlattice.[9] The cluster Green's functions and self-energies are now matrices of size $n_c \times n_c$, while ϵ_k becomes a matrix $\hat{v}(k)$, defined as the Fourier transform of the hopping matrix on the superlattice. The momenta k are those of the reduced Brillouin zone of the superlattice.

To be more specific, let us consider a one-dimensional Hubbard chain, with lattice spacing a, that we decompose into two-site clusters. The hopping matrix then has the form

$$\left(\begin{array}{c|cc|cc|c} \ddots & -v & & & & \\ \hline -v & 0 & -v & & & \\ & -v & 0 & -v & & \\ \hline & & -v & 0 & -v & \\ & & & -v & 0 & -v \\ \hline & & & & -v & \ddots \end{array}\right),$$

which after Fourier transformation on the superlattice with spacing $2a$ becomes

$$-\hat{v}(k) = e^{ik0}\begin{pmatrix} 0 & v \\ v & 0 \end{pmatrix} + e^{ik(2a)}\begin{pmatrix} 0 & 0 \\ v & 0 \end{pmatrix} + e^{ik(-2a)}\begin{pmatrix} 0 & v \\ 0 & 0 \end{pmatrix}$$
$$= \begin{pmatrix} 0 & v(1+e^{-i2ka}) \\ v(1+e^{i2ka}) & 0 \end{pmatrix}. \tag{18}$$

The self-consistency condition, which fixes the 2×2 matrix of the dynamical mean field $\mathcal{G}_0$ or Δ, is now

$$\int_{\text{reduced BZ}} (dk)[(i\omega_n + \mu)\hat{I} - \hat{v}(k) - \hat{\Sigma}_{\text{imp}}(i\omega_n)]^{-1} = \hat{G}_{\text{imp}}, \tag{19}$$

with the reduced Brillouin zone $-\pi/2a \leq k < \pi/2a$.

As is evident from the hopping matrix (18), the cluster DMFT formalism breaks translational invariance within the cluster. There is an alternative cluster DMFT, called the *dynamical cluster approximation*, which enforces this symmetry.[8] The two-site DCA corresponds to the hopping matrix

$$-\hat{v}_{DCA}(k) = \begin{pmatrix} 0 & 2v\cos(ka) \\ 2v\cos(ka) & 0 \end{pmatrix}. \tag{20}$$

In the "momentum basis," $\{d_{K=0} = \frac{1}{\sqrt{2}}(d_1 + d_2), d_{K=\frac{\pi}{a}} = \frac{1}{\sqrt{2}}(d_1 - d_2)\}$, the Green's functions and self-energies are diagonal matrices, and the self-consistency conditions for each "momentum sector" K is

$$\int_{\text{sector } K} (dk)[i\omega_n + \mu - \epsilon_k - \Sigma^K_{\text{imp}}(i\omega_n)]^{-1} = G^K_{\text{imp}}, \tag{21}$$

with $\epsilon_k = -2v\cos(ka)$. In our two-site example, sector $K = 0$ corresponds to $-\pi/2a \leq k < \pi/2a$, while sector $K = \pi/a$ corresponds to $\pi/2a \leq k < 3\pi/2a$. The first Brillouin zone thus decomposes into two sectors of equal size, centered at the reciprocal lattice vectors of the periodized two-site cluster.

III. NONEQUILIBRIUM GENERALIZATION

A. Kadanoff-Baym contour

Let us consider a Hubbard model with time-dependent parameters,

$$H(t) = -\sum_{\langle ij\rangle\sigma} v_{ij}(t)(d^\dagger_{i\sigma}d_{j\sigma} + d^\dagger_{j\sigma}d_{i\sigma}) + U(t)\sum_i n_{i\uparrow}n_{i\downarrow} - \mu(t)\sum_{i\sigma} n_{i\sigma}. \tag{22}$$

Initially (at $t = 0$) the system is assumed to be in an equilibrium state at inverse temperature $\beta = 1/T$, and thus described by the density matrix

$$\rho(0) = \frac{1}{Z} e^{-\beta H(0)}, \tag{23}$$

where $Z = \mathrm{Tr}\, e^{-\beta H(0)}$ is the equilibrium partition function. The time evolution of the density matrix is determined by the von Neumann equation,

$$i\frac{d}{dt}\rho(t) = [H(t), \rho(t)], \tag{24}$$

where the bracket represents the commutator. Formally, one can write the solution of Eq. (24) as

$$\rho(t) = U(t,0)\,\rho(0)\,U(0,t), \tag{25}$$

with the time-evolution operator defined as

$$U(t,t') = \begin{cases} \mathcal{T} \exp\left(-i \displaystyle\int_{t'}^{t} d\bar{t}\, H(\bar{t})\right) & t > t', \\ \tilde{\mathcal{T}} \exp\left(-i \displaystyle\int_{t'}^{t} d\bar{t}\, H(\bar{t})\right) & t < t'. \end{cases} \tag{26}$$

Here $\mathcal{T}$ ($\tilde{\mathcal{T}}$) denotes the (anti-)time-ordering operator. Note that the Hamiltonians at different times do in general not commute ($[H(t), H(t')] \neq 0$). With this ordering, the evolution operator becomes unitary, $U(t,t')[U(t,t')]^\dagger = 1$, and satisfies $U(t,t')U(t',t'') = U(t,t'')$.

Using the time-dependent density matrix (25), the expectation value of an observable $\mathcal{O}$ measured at time t is given by

$$\langle \mathcal{O}(t) \rangle = \mathrm{Tr}\,[\rho(t)\mathcal{O}]. \tag{27}$$

By substituting $\rho(0)$ defined in Eq. (23) into Eq. (25) and interpreting $e^{-\beta H(0)} \equiv U(-i\beta, 0)$ as the evolution along the imaginary time axis from 0 to $-i\beta$ (with imaginary-time ordering), we can express Eq. (27) as

$$\langle \mathcal{O}(t) \rangle = \frac{1}{Z}\mathrm{Tr}\,[U(t,0)e^{-\beta H(0)}U(0,t)\mathcal{O}] = \frac{1}{Z}\mathrm{Tr}\,[U(-i\beta,0)U(0,t)\mathcal{O}U(t,0)]. \tag{28}$$

In the last step, we have permuted the operators under the trace. The operators, read from right to left, follow the time ordering $0 \to t \to 0 \to -i\beta$. It is thus convenient to introduce the L-shaped contour $\mathcal{C}$ with the three branches $\mathcal{C}_1$: $0 \to t_{\max}$, $\mathcal{C}_2$: $t_{\max} \to 0$, and

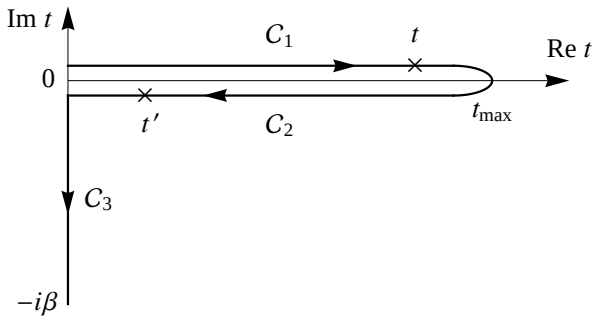

FIG. 2: The L-shaped contour $\mathcal{C} = \mathcal{C}_1 \cup \mathcal{C}_2 \cup \mathcal{C}_3$ in the Kadanoff-Baym formalism. The arrows indicate the contour ordering. For example, t' lies ahead of t in the contour ordering. (From Ref. 5.)

$\mathcal{C}_3$: $0 \to -i\beta$, as shown in Fig. 2, where $t_{\max}$ is the maximum time up to which one wants to let the system evolve. Then the expectation value (28) can be written as

$$\langle \mathcal{O}(t) \rangle = \frac{1}{Z} \mathrm{Tr}\Big[\mathcal{T}_{\mathcal{C}}\, e^{-i \int_{\mathcal{C}} d\bar{t}\, H(\bar{t})} \mathcal{O}(t) \Big] = \frac{\mathrm{Tr}\big[\mathcal{T}_{\mathcal{C}}\, e^{-i \int_{\mathcal{C}} d\bar{t}\, H(\bar{t})} \mathcal{O}(t) \big]}{\mathrm{Tr}\big[\mathcal{T}_{\mathcal{C}}\, e^{-i \int_{\mathcal{C}} d\bar{t}\, H(\bar{t})} \big]}, \tag{29}$$

where $\mathcal{T}_{\mathcal{C}}$ is the contour-ordering operator that arranges operators on the contour $\mathcal{C}$ in the order $0 \to t_{\max} \to 0 \to -i\beta$ (as indicated by the arrows in Fig. 2), $\mathcal{O}(t)$ indicates that the operator $\mathcal{O}$ is inserted at time t on the contour $\mathcal{C}$, and we have used the fact that the evolution along the forward ($\mathcal{C}_1$) and backward ($\mathcal{C}_2$) contours cancels if no other operator is inserted, so that $e^{-\beta H(0)} = \mathcal{T}_{\mathcal{C}} \exp\big(-i \int_{\mathcal{C}} d\bar{t}\, H(\bar{t})\big)$.

The contour-ordered formalism can also be applied to higher-order correlation functions,

$$\langle \mathcal{T}_{\mathcal{C}}\, \mathcal{A}(t) \mathcal{B}(t') \rangle \equiv \frac{1}{Z} \mathrm{Tr}\left[\mathcal{T}_{\mathcal{C}}\, e^{-i \int_{\mathcal{C}} d\bar{t}\, H(\bar{t})} \mathcal{A}(t) \mathcal{B}(t') \right]. \tag{30}$$

In this expression, t and t' can lie anywhere on $\mathcal{C}$, and the contour-ordered product of two operators $\mathcal{A}$ and $\mathcal{B}$ is defined as $\mathcal{T}_{\mathcal{C}}\, \mathcal{A}(t)\mathcal{B}(t') = \theta_{\mathcal{C}}(t,t')\mathcal{A}(t)\mathcal{B}(t') \pm \theta_{\mathcal{C}}(t',t)\mathcal{B}(t')\mathcal{A}(t)$, where $\theta_{\mathcal{C}}(t,t') = 1$ when t' comes earlier than t in the contour ordering and 0 otherwise. The sign $\pm$ is minus when the operators $\mathcal{A}$ and $\mathcal{B}$ are both fermionic and plus otherwise. Whenever an operator is subject to the contour-ordered product, one has to specify which branch its time argument lies on.

Of particular relevance are the contour-ordered nonequilibrium Green's functions, which we define as

$$G(t,t') \equiv -i \langle \mathcal{T}_{\mathcal{C}}\, d(t)\, d^{\dagger}(t') \rangle, \tag{31}$$

where $t, t' \in \mathcal{C}$. For simplicity, spin and orbital indices associated with the operators are not shown. Due to the three branches, on which the time arguments t and t' can lie, the Green's function has $3 \times 3 = 9$ components: $G(t,t') \equiv G_{ij}(t,t')$ ($t \in \mathcal{C}_i$, $t' \in \mathcal{C}_j$, $i,j = 1,2,3$). Conventionally we express them in a 3×3 matrix form,

$$\hat{G} = \begin{pmatrix} G_{11} & G_{12} & G_{13} \\ G_{21} & G_{22} & G_{23} \\ G_{31} & G_{32} & G_{33} \end{pmatrix}. \tag{32}$$

B. Dynamical mean field formalism

Since the dynamical mean field formalism only involves an approximation on the spatial degrees of freedom (the mapping from a lattice model to a single-site or cluster impurity model), while time-dependent fluctuations are retained, it is conceptually rather easy to extend this formalism to nonequilibrium situations. All we have to do is to solve the DMFT equations on the L-shaped Kadanoff-Baym contour (Fig. 2), instead of solving them on the imaginary-time interval (which corresponds to the branch $\mathcal{C}_3$ of this contour). However, because we do not in general have time-translation invariance anymore, the Green's function $G(t,t')$, self-energy $\Sigma(t,t')$, and hybridization function $\Delta(t,t')$ depend on two time-arguments t and t', rather than just the time difference $t-t'$, and we cannot solve the DMFT equations by Fourier transformation anymore. They become coupled integral-differential equations for the different components of the respective 3×3 matrices.

We can define a nonequilibrium Anderson impurity model by the contour action

$$S_{\rm imp} = S_{\rm loc} + S_{\rm hyb} = -i \int_{\mathcal{C}} dt\, H_{\rm loc}(t) - i \sum_{\sigma} \int_{\mathcal{C}} dt\, dt'\, d^{\dagger}_{\sigma}(t) \Delta(t,t') d_{\sigma}(t'), \tag{33}$$

where $H_{\rm loc}(t)$ denotes the interaction and chemical potential terms in Eq. (22), and $\Delta(t,t')$ is a hybridization function defined on the contour. With this, the contour-ordered impurity Green's function is defined as

$$G_{\rm imp}(t,t') = -i \langle \mathcal{T}_{\mathcal{C}}\, d(t) d^{\dagger}(t') \rangle_{S_{\rm imp}}, \tag{34}$$

where the expectation value of observables with respect to $S_{\rm imp}$ is

$$\langle \cdots \rangle_{S_{\rm imp}} = \frac{{\rm Tr}[\mathcal{T}_{\mathcal{C}}\, \exp(S_{\rm imp}) \cdots]}{{\rm Tr}[\mathcal{T}_{\mathcal{C}}\, \exp(S_{\rm imp})]}. \tag{35}$$

The hybridization function $\Delta(t,t')$, or equivalently the Weiss Green's function

$$\mathcal{G}_0(t,t') = (i\partial_t + \mu(t))\delta_{\mathcal{C}}(t,t') - \Delta(t,t') \tag{36}$$

plays the role of the dynamical mean field and is fixed by the usual self-consistency loop (now to be solved on the contour $\mathcal{C}$):

1. Solve the impurity problem, that is, compute the impurity Green's function $G_{\rm imp}(t,t')$ for the given $\mathcal{G}_0(t,t')$,

2. Extract the self-energy of the impurity model: $\Sigma_{\rm imp}(t,t') = \mathcal{G}_0^{-1}(t,t') - G_{\rm imp}^{-1}(t,t')$,

3. Identify the lattice self-energy with the impurity self-energy, $\Sigma_k(t,t') = \Sigma_{\rm imp}(t,t')$ (DMFT approximation), and compute the local lattice Green's function $G_{\rm loc}(t,t') = \int (dk)[(i\partial_t + \mu(t) - \epsilon_k(t))\delta_{\mathcal{C}}(t,t') - \Sigma_{\rm imp}(t,t')]^{-1}$ $(= \int (dk)[G_{0,k}^{-1}(t,t') - \Sigma_{\rm imp}(t,t')]^{-1})$,

4. Apply the DMFT self-consistency condition, $G_{\rm loc}(t,t') = G_{\rm imp}(t,t')$, and use it to define a new Weiss Green's function: $\mathcal{G}_0^{-1}(t,t') = G_{\rm loc}^{-1}(t,t') + \Sigma_{\rm imp}(t,t')$.

In order to appreciate the meaning of these formal expressions, we have to add some explanations.

a. Noninteracting Green's functions. The noninteracting lattice Green's function $G_{0,k}(t,t') = -i\langle \mathcal{T}_{\mathcal{C}} d_k(t) d_k^\dagger(t')\rangle$ for $H_0(t) = \sum_k [\epsilon_k(t) - \mu(t)] d_k^\dagger d_k$ satisfies

$$\big[i\partial_t + \mu(t) - \epsilon_k(t)\big] G_{0,k}(t,t') = \delta_{\mathcal{C}}(t,t'), \tag{37a}$$

$$G_{0,k}(t,t')\big[-i\overleftarrow{\partial_{t'}} + \mu(t') - \epsilon_k(t')\big] = \delta_{\mathcal{C}}(t,t'), \tag{37b}$$

where $g(t)\overleftarrow{\partial_t} \equiv \partial_t g(t)$. The two equations are equivalent, and each determines $G_{0,k}$ uniquely if solved with the boundary condition $G(0^+,t) = -G(-i\beta,t)$, $G(t,0^+) = -G(t,-i\beta)$:

$$G_{0,k}(t,t') = -i[\theta_{\mathcal{C}}(t,t') - f(\epsilon_k(0) - \mu(0))] e^{-i\int_{t'}^t d\bar{t}[\epsilon_k(\bar{t}) - \mu(\bar{t})]}, \tag{38}$$

where $f(\epsilon) = 1/(e^{\beta\epsilon} - 1)$ is the Fermi occupation function. The two equations of motion (37) can be rewritten by introducing the inverse of the Green's function

$$G_{0,k}^{-1}(t,t') = \big[i\partial_t + \mu(t) - \epsilon_k(t)\big]\delta_{\mathcal{C}}(t,t'), \tag{39}$$

which is a differential operator on the contour. Equations (37) then simply read $G_{0,k}^{-1} * G_{0,k} = G_{0,k} * G_{0,k}^{-1} = \delta_{\mathcal{C}}$, where the star denotes a contour convolution.

The noninteracting impurity Green's function is given by Eq. (36).

b. Dyson equation The interacting Green's function G is given by the Dyson equation,

$$G = G_0 + G_0 * \Sigma * G \tag{40}$$

$$= G_0 + G * \Sigma * G_0. \tag{41}$$

We can transform the Dyson equation and its conjugate from its integral form into a differential form by convoluting with the operator G_0^{-1} from the left [Eq. (40)] or right [Eq. (41)], respectively,

$$[G_0^{-1} - \Sigma] * G = G * [G_0^{-1} - \Sigma] = \delta_{\mathcal{C}}. \tag{42}$$

The result may be expressed as $G^{-1} = G_0^{-1} - \Sigma$, which looks identical to the equilibrium form of the Dyson equation. However, Eq. (42) has a different meaning for Matsubara and contour-ordered Green's functions. In the nonequilibrium case, the two Eqs. (42) are integro-differential equations of the form

$$[i\partial_t + \mu(t) - \epsilon_k(t)]G(t,t') - \int_{\mathcal{C}} d\bar{t}\, \Sigma(t,\bar{t})G(\bar{t},t') = \delta_{\mathcal{C}}(t,t'), \tag{43a}$$

$$G(t,t')[-i\overleftarrow{\partial_{t'}} + \mu(t') - \epsilon_k(t')] - \int_{\mathcal{C}} d\bar{t}\, G(t,\bar{t})\Sigma(\bar{t},t') = \delta_{\mathcal{C}}(t,t'). \tag{43b}$$

The time derivative $\partial_t G$ in these equations is related to the value of G at different times via the convolution $\Sigma * G$. The equations are causal, and define a time-propagation scheme for G, in which the self-energy plays the role of a memory kernel. On the imaginary branch, on the other hand, the same equations provide a boundary value problem for the (Matsubara) Green's functions of an equilibrium state, which can be solved by Fourier transformation. This equilibrium solution provides the initial value for the time propagation.

c. Time-dependent electric fields. The first term in Eq. (22), with arbitrary hoppings $v_{ij}(t)$, can incorporate the effect of time-dependent electromagnetic fields. For a single-band model, the Peierls substitution[10] introduces the vector potential $A(r,t)$ as a phase factor in the hopping matrix elements,

$$v_{ij}(t) = v_{ij} \exp\left(-ie \int_{R_i}^{R_j} dr\, A(r,t)\right), \tag{44}$$

and adds a scalar potential term $e\sum_{i\sigma} \Phi(R_i,t) d_{i\sigma}^\dagger d_{i\sigma}$ to the Hamiltonian (e is the charge of an electron). It derives from the requirement that the Hamiltonian is invariant under the

gauge transformation

$$d_{j\sigma} \to d_{j\sigma} \exp\Big(ie\,\chi(R_j,t)\Big), \tag{45a}$$

$$A(r,t) \to A(r,t) + \nabla\chi(r,t), \tag{45b}$$

$$\Phi(r,t) \to \Phi(r,t) - \frac{\partial\chi(r,t)}{\partial t}. \tag{45c}$$

The (gauge-invariant) current operator can then be obtained from the derivative $j(r) = -\delta H/\delta A(r)$. Usually, we consider situations in which the applied field varies only slowly on the atomic scale, which is well satisfied even for optical frequencies. When the r-dependence of A is neglected, the Peierls substitution leads to a time-dependent dispersion

$$\epsilon_k(t) = \epsilon(k - eaA(t)), \tag{46}$$

where $\epsilon(k)$ is the dispersion for zero field, and a is the lattice spacing, so that the hopping part of the Hamiltonian reads $H_0 = \sum_{k\sigma} \epsilon_k(t)\, n_{k\sigma}$. Correspondingly, the current operator in the limit of long wavelengths becomes

$$j(t) = \frac{e}{V} \sum_{k\sigma} \mathcal{V}_k(t) n_{k\sigma}, \tag{47}$$

where V is the volume, and $\mathcal{V}_k$ is the group velocity of the Bloch electrons,

$$\mathcal{V}_k(t) = \partial_k \epsilon_k(t) = \partial_k \epsilon(k - eaA(t)). \tag{48}$$

IV. SPECTROSCOPY

As a Green's function based method, DMFT gives access to the occupation of the many-body states and the excitation spectrum. In order to discuss how this information can be extracted in the nonequilibrium context, we have to take a closer look at the 3×3 components of the contour Green's function (32). In general, one can shift the operator with the largest real-time argument (e.g., t in Fig. 2) from $\mathcal{C}_1$ to $\mathcal{C}_2$ (and vice versa), because the time-evolution along $\mathcal{C}_1$ and $\mathcal{C}_2$ to the right of that operator cancels. This kind of redundancy

implies the following relations among the components of the matrix (32),

$$G_{11}(t,t') = G_{12}(t,t') \quad (\text{for } t \le t'), \tag{49a}$$

$$G_{11}(t,t') = G_{21}(t,t') \quad (\text{for } t > t'), \tag{49b}$$

$$G_{22}(t,t') = G_{21}(t,t') \quad (\text{for } t < t'), \tag{49c}$$

$$G_{22}(t,t') = G_{12}(t,t') \quad (\text{for } t \ge t'), \tag{49d}$$

$$G_{13}(t,\tau') = G_{23}(t,\tau'), \tag{49e}$$

$$G_{31}(\tau,t') = G_{32}(\tau,t'). \tag{49f}$$

These relations allow one to eliminate three of the nine components in the Green's function (32), and to introduce six linearly independent "physical" Greens functions, called the retarded (G^R), advanced (G^A), Keldysh (G^K), left-mixing ($G^{\urcorner}$), right-mixing ($G^{\ulcorner}$), and Matsubara Green's function (G^M). They are explicitly given by

$$G^R(t,t') = \tfrac{1}{2}(G_{11} - G_{12} + G_{21} - G_{22}) = -i\theta(t-t')\langle\{d(t), d^\dagger(t')\}\rangle, \tag{50a}$$

$$G^A(t,t') = \tfrac{1}{2}(G_{11} + G_{12} - G_{21} - G_{22}) = i\theta(t'-t)\langle\{d(t), d^\dagger(t')\}\rangle, \tag{50b}$$

$$G^K(t,t') = \tfrac{1}{2}(G_{11} + G_{12} + G_{21} + G_{22}) = -i\langle[d(t), d^\dagger(t')]\rangle, \tag{50c}$$

$$G^{\urcorner}(t,\tau') = \tfrac{1}{2}(G_{13} + G_{23}) = i\langle d^\dagger(\tau')d(t)\rangle, \tag{50d}$$

$$G^{\ulcorner}(\tau,t') = \tfrac{1}{2}(G_{31} + G_{32}) = -i\langle d(\tau)d^\dagger(t')\rangle, \tag{50e}$$

$$G^M(\tau,\tau') = -iG_{33} = -\langle \mathcal{T}_\tau\, d(\tau)d^\dagger(\tau')\rangle. \tag{50f}$$

In the above formulas, we assume fermionic operators d and $d^\dagger$, $[,]$ $(\{,\})$ denotes a commutator (anti-commutator), $t, t' \in \mathcal{C}_1 \cup \mathcal{C}_2$, $\tau, \tau' \in \mathcal{C}_3$, $\theta(t)$ is the step function, and $\mathcal{T}_\tau$ is the time-ordering operator on the imaginary time axis. Note that the commutator is used for fermionic operators in G^K (50c). For convenience, we also define the lesser and greater Green's functions

$$G^<(t,t') = G_{12} = i\langle d^\dagger(t')d(t)\rangle, \tag{50g}$$

$$G^>(t,t') = G_{21} = -i\langle d(t)d^\dagger(t')\rangle, \tag{50h}$$

which are related to the retarded, advanced, and Keldysh Green's functions via

$$G^< = \tfrac{1}{2}(G^K - G^R + G^A), \tag{51a}$$

$$G^> = \tfrac{1}{2}(G^K + G^R - G^A). \tag{51b}$$

The physical components (50) are useful for the interpretation of simulation results. We can motivate this by first considering the equilibrium case. When H does not depend on time, the real-time components of $G(t,t')$ depend on the time difference $t-t'$ only and can be Fourier transformed. The imaginary part of the retarded (or advanced) Green's function gives the single-particle spectral function,[11]

$$A(\omega) = -\frac{1}{\pi}\mathrm{Im}\, G^R(\omega) = \frac{1}{\pi}\mathrm{Im}\, G^A(\omega), \tag{52}$$

which represents the density of single-particle excitations at energy ω of the many-body state, as can be seen from the Lehmann representation,[12]

$$A(\omega) = \frac{1}{Z}\sum_{mn}\left(e^{-\beta E_n} + e^{-\beta E_m}\right)|\langle n|c^\dagger|m\rangle|^2\delta(\omega - E_n + E_m). \tag{53}$$

Out of equilibrium, one can still define the spectral function using the partial Fourier transformation [$t_{\mathrm{av}} = (t+t')/2$, $t_{\mathrm{rel}} = t-t'$],

$$A(\omega, t_{\mathrm{av}}) = -\frac{1}{\pi}\mathrm{Im}\int dt_{\mathrm{rel}} e^{i\omega t_{\mathrm{rel}}} G^R(t,t'), \tag{54}$$

which satisfies the sum rule $\int d\omega A(\omega, t_{\mathrm{av}}) = 1$.

In equilibrium, all components of G can be related to the spectral function by

$$G(t,t') = -i\int d\omega\, e^{i\omega(t'-t)}\, A(\omega)\,[\theta_{\mathcal{C}}(t,t') - f(\omega)]. \tag{55}$$

Since the contour step function is 0 (1) for the lesser (greater) Green's function G_{12} (G_{21}), this expression relates the imaginary parts of these Green's functions to the density of *occupied* (*unoccupied*) states,

$$\mathrm{Im}\, G^<(\omega) = 2\pi\, A(\omega) f(\omega) \equiv 2\pi N(\omega), \tag{56a}$$

$$-\mathrm{Im}\, G^>(\omega) = 2\pi\, A(\omega)[1 - f(\omega)]. \tag{56b}$$

In equilibrium, the density of occupied (unoccupied) states is often calculated to understand (inverse) photoemission spectroscopy in correlated materials. Similarly, intensities for time-resolved (inverse) photoemission spectroscopy can be obtained from the real-time Green's functions $G^<(t,t')$ and $G^>(t,t')$.

Static photoemission spectroscopy in equilibrium is often analyzed in terms of the momentum-resolved spectral function,

$$I(k_f, E) = \sum_k |M_k|^2 \delta_{k_\parallel + q_\parallel, k_{f\parallel}}\, N_k(E - \hbar\omega_q - W), \tag{57}$$

where $N_k(\omega) = f(\omega)A_k(\omega)$ is the occupied density of states at momentum k [cf. Eq. (56a)], q is the momentum of the incoming photon, and $I(k_f, E)$ is the photoemission intensity at final momentum k_f and energy E. The delta function accounts for momentum conservation parallel to the surface, and the M_k denote matrix elements, which are usually approximated as k-independent. The most important approximation entering this expression is the so-called sudden approximation,[13] which neglects interactions between the outgoing electron and the bulk and thus allows to express the photoelectron current in terms of single-particle properties of the sample.

In time-resolved ARPES one probes the state of a system with a short pulse with center-frequency Ω, and counts the total number of electrons emitted with a certain momentum k_f and energy E. The electric field of the probe pulse is of the form $\cos[\Omega(t - t_p + \phi)]S(t - t_p)$, where $S(t)$ is the probe envelope, t_p is the probing time, and ϕ is the carrier-envelope phase. The system can be in an arbitrary nonequilibrium state due to an earlier perturbation (for example a pump excitation). Equation (57) can be generalized to this situation:[14] In the sudden approximation, the electric probe field couples the electronic orbitals in the sample to the outgoing electron states $|k_f\rangle$ via some dipole matrix element. If we disregard the k-dependence of this matrix element, second-order time-dependent perturbation theory gives (after averaging over the carrier-envelope phase ϕ)

$$I(k_f, E; t_p) \propto \sum_k \delta_{k_\parallel + q_\parallel, k_{f\parallel}} I_k(E - \hbar\omega_q - W; t_p), \tag{58}$$

$$I_k(\omega; t_p) = -i \int dt dt'\, S(t)S(t') e^{i\omega(t'-t)} G_k^<(t + t_p, t' + t_p). \tag{59}$$

This expression connects the ARPES measurement to the contour Green's functions determined in DMFT. (In contrast, the imaginary part of a partial Fourier transform $G^<(\omega, t) = \int d\bar{t} e^{i\omega\bar{t}} G^<(t + \bar{t}/2, t - \bar{t}/2)$ is not always positive.) The equation contains the fundamental frequency-time uncertainty:[15] When the probe pulse is very short, $S(t) = \delta(t)$, one measures instantaneous occupations $G_k^<(t, t) = n_k(t)$, but all energy resolution is lost. In the limiting case of a stationary state, Eq. (59) reduces to a convolution of the equilibrium result (57) with the spectral density $|\tilde{S}(\omega)|^2$ of the probe pulse.

V. APPLICATIONS

A. AC field quench

In the introduction, we have mentioned that one of the goals in the study of nonequilibrium condensed matter systems is to "tune" material properties by driving a correlated electron system out of equilibrium, for example by applying strong electric fields. Here, we present a nonequilibrium DMFT calculation of a one-band Hubbard model driven by periodic fields,[16] which provides a glimpse of the type of phenomena that can be expected to occur in driven systems. One remarkable prediction is that it is not only possible to tune the strength of the effective Coulomb repulsion by external driving, but that under suitable conditions, the repulsive interaction can be switched into an attractive interaction between electrons.

We consider a half-filled Hubbard model on an infinite-dimensional hypercubic lattice and a field $\boldsymbol{E}(t) = \boldsymbol{E}\cos(\Omega t)$ with polarization in the body diagonal ($\boldsymbol{E} = E(1, 1, \ldots, 1)$). In this case the hopping v_{ij} is renormalized by the periodic driving to an effective hopping parameter[17]

$$v_{ij}^{\text{eff}} = \mathcal{J}_0(E/\Omega)\, v_{ij}, \tag{60}$$

where $\mathcal{J}_0$ is the zeroth-order Bessel function. The Bessel function is an oscillating function with sign changes (see right hand panel of Fig. 3). When $\mathcal{J}_0(E/\Omega) = 0$, Eq. (60) implies that the effective hopping vanishes (dynamical localization). As we will see below, the consequences of $\mathcal{J}_0(E/\Omega) < 0$ are even more interesting.

We can understand the relation (60) by choosing a gauge with pure vector potential, $\boldsymbol{E} = \partial_t \boldsymbol{A}$, with $\boldsymbol{A}(t) = -\boldsymbol{E}\sin(\Omega t)/\Omega$. The Peierls substitution (46) then yields a time-dependent dispersion $\epsilon_{\boldsymbol{k}-\boldsymbol{A}(t)}$ (we set e and a to 1 in the following). Averaging this dispersion over one period of the driving field gives

$$\overline{\epsilon_{\boldsymbol{k}}} = \frac{\Omega}{2\pi}\int_0^{2\pi/\Omega} dt \epsilon_{\boldsymbol{k}-\boldsymbol{A}(t)} = \mathcal{J}_0(E/\Omega)\epsilon_{\boldsymbol{k}}. \tag{61}$$

Let us consider what happens when the ac field is suddenly switched on at $t = 0$. Figure 3 shows the result for the double occupancy $D(t) = \langle \hat{n}_\uparrow(t)\hat{n}_\downarrow(t)\rangle$ for various values of E/Ω with a fixed Ω. Initially D is smaller than the noninteracting value $\langle \hat{n}_\uparrow\rangle\langle \hat{n}_\downarrow\rangle = 0.25$ due to the repulsive interaction. The switch-on of an ac field with small amplitude leads to a

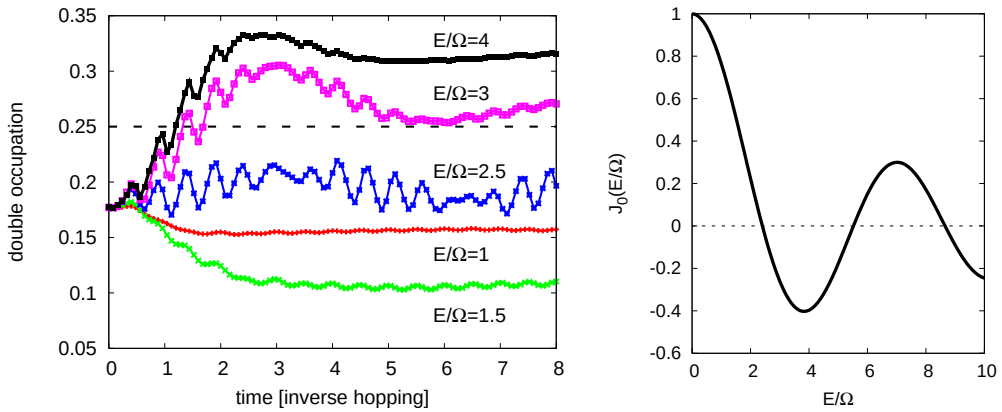

FIG. 3: Left panel: Time evolution of the double occupancy after an ac field quench with amplitude E and frequency Ω. The interaction is $U = 1$. Right panel: Bessel function $\mathcal{J}_0(E/\Omega)$ with sign changes at $E/\Omega = 2.4, 5.5, \ldots$. (Adapted from Ref. 16.)

decrease of D, accompanied by rapid oscillations with frequency 2Ω due to the nonlinear effect of the ac field. The suppression of D can be interpreted as an enhanced U/W due to the hopping renormalization (60) [W is the bandwidth, here the width of the Gaussian density of states of the infinite-dimensional hypercubic lattice].

In a half-filled equilibrium system with repulsive interactions, $D \leq 0.25$ (the equal sign holds in the limit of infinite temperature). Remarkably, the double occupancy in Fig. 3 *exceeds* 0.25 when $\mathcal{J}_0(E/\Omega) < 0$. This implies that the many-body interaction has turned into an effective attraction ($U_{\rm eff} < 0$). The origin of this sign inversion is a dynamical band flipping.[16] If the field is ramped up quickly, the occupation in momentum space does not change significantly, resulting in a population inversion, or "negative temperature" ($T_{\rm eff} < 0$) occupation in the flipped band (Fig. 4).

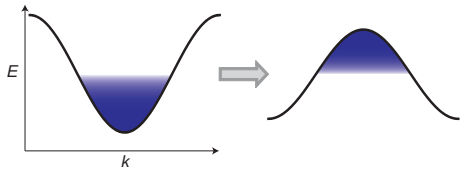

FIG. 4: Schematic picture of the dynamical band flipping with population inversion induced by an ac field quench with $\mathcal{J}_0(E/\Omega) < 0$. (From Ref. 5).

If we look at the time-dependent density matrix of this state, we have

$$\rho(t) \sim e^{-[\mathcal{J}_0(E/\Omega)H_0+H_{\rm int}]/T_{\rm eff}} = e^{-[H_0+H_{\rm int}/\mathcal{J}_0(E/\Omega)][T_{\rm eff}/\mathcal{J}_0(E/\Omega)]}. \tag{62}$$

In other words, a positive (repulsive) U in a negative T state is equivalent to a negative (attractive) U in a positive T state. Hence, the ac-field quench amounts to an interaction quench,

$$U \to U_{\rm eff} = U/\mathcal{J}_0(E/\Omega). \tag{63}$$

The ac-field quench provides a new way of inducing attractive interactions between electrons. It may lead to an s-wave superconducting state with high T_c.

B. Nonthermal long-range ordered states

Correlated lattice systems exhibit various types of long-range order, including antiferromagnetism, superconductivity, and charge order. A symmetry-broken state on a bipartite lattice can be treated within DMFT by solving impurity problems for each sublattice.[6] The impurity model for sublattice A is fixed by the local Green's function on sublattice B and vice versa. Here, we will consider antiferromagnetic order and a semielliptic density of states of bandwidth $4v$, for which the DMFT self-consistency condition can be expressed in a closed form: the hybridization function $\Delta_{A,\sigma}$ ($\Delta_{B,\sigma}$) for the A (B) sublattice is given by $\Delta_{A,\sigma} = v^2 G_{B,\sigma}$ ($\Delta_{B,\sigma} = v^2 G_{A,\sigma}$), where G is the local lattice Green's function. Together with the relation $\Delta_{A,\sigma} = \Delta_{B,\bar{\sigma}}$ for pure Néel-type symmetry breaking, this leads to a single impurity calculation with the self-consistency condition $\Delta_\sigma = v^2 G_{\bar{\sigma}}$.

The DMFT phase diagram for the half-filled, repulsive Hubbard model exhibits an antiferromagnetically ordered insulating phase at low temperature (Fig. 5). For attractive U, one finds an analogous phase diagram with AFM order replaced by s-wave superconductivity[18] (at half-filling the superconducting state is degenerate with a charge ordered phase due to a symmetry between the repulsive and attractive models,[19] but in the doped system, superconductivity is more stable). The nature of the AFM insulating (or s-wave superconducting) state changes qualitatively as $|U|$ crosses the value corresponding roughly to the maximum in the critical temperature. This is known as the "BCS-BEC" crossover in the literature on cold atomic gases.

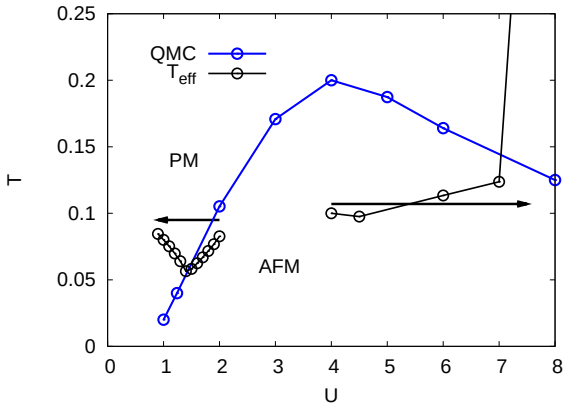

FIG. 5: Antiferromagnetic phase diagram for the half-filled Hubbard model (semi-elliptic DOS, bandwidth 4; QMC data from Ref. 20). The black dots show the effective temperatures after quenches from $U_i = 2$, $T = 0.08$ to $U_f = 1.9, 1.8, \ldots, 1.0$, and for quenches from $U_i = 4$, $T = 0.1$ to $U_f = 6, 7, 8$.

First, we consider the time evolution of the magnetization m after interaction quenches (more precisely ramps) out of the antiferromagnetic phase on the weak-coupling side. Starting from $T \approx 0.08$, $U_i = 2$ we rapidly change the interaction to $U_f = 1.9, 1.8, \ldots, 1.0$.[21] Interaction quenches may seem far-fetched in the condensed matter context, but in the previous section we have discussed a theoretical proposal how this may be realized in driven systems. Here, we just use the interaction quenches as a convenient method to drive the system across the phase boundary into the disordered state. We expect to see the same phenomena if the system crosses the phase boundary along the temperature axis, for example after the injection of energy through an electric field pulse.

The left-hand panel of Fig. 6 shows the time evolution of the magnetization after the quench. The arrows indicate the values of the magnetization expected for the thermalized state in the long-time limit. The thermal magnetization, which can be calculated independently from the energy injected into the system by the quench, becomes zero for $U_f \leq U_{c,\mathrm{thermal}} = 1.42$. Remarkably, however, even for some $U_f \leq U_{c,\mathrm{thermal}}$, the order parameter shows coherent oscillations ("amplitude mode") around a non-zero value, followed by a slow decay. If we plot the frequency of the amplitude oscillations as a function of U_f (see middle panel), we find a roughly linear curve which extrapolates to zero at $U_f \approx 1.22$. This suggests that a nonthermal magnetized state persists up to some "nonthermal critical

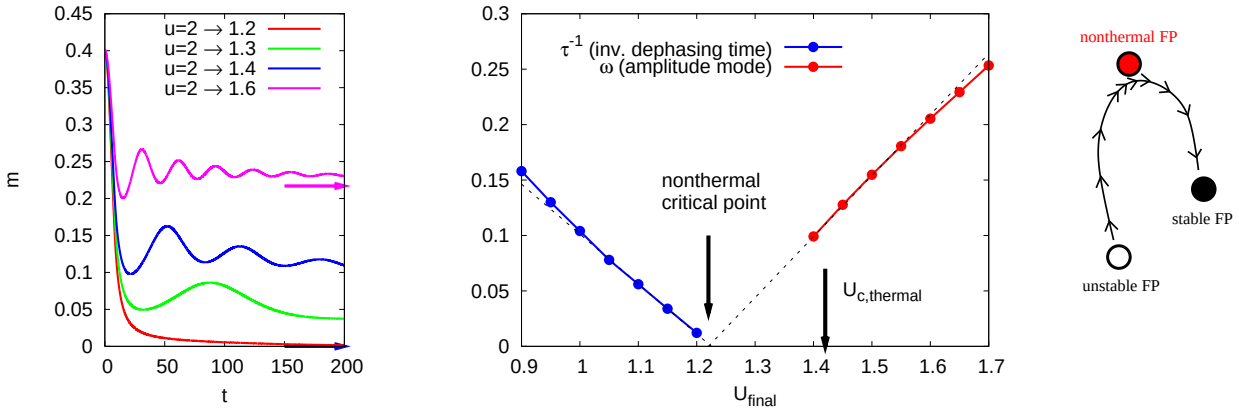

FIG. 6: Quench out of the antiferromagnetic phase in the weak-coupling regime. Left panel: Time evolution of the magnetization after a quench from $U_i = 2$, $T = 0.08$ to $U_f = 1.6, 1.4, 1.3, 1.2$. For $U_f \leq U_{c,\mathrm{thermal}} = 1.42$, the system will thermalize in the paramagnetic phase. Middle panel: Frequency of the amplitude mode and inverse dephasing time as a function of U_f. The corresponding time-scales diverge near $U_f \approx 1.22$ ("nonthermal critical point"). Right panel: Sketch of the "RG flow" after the quench, from the unstable antiferromagnetic fixed point (FP) to the stable paramagnetic fixed point. At intermediate times, the properties of the system are controlled by a nonthermal "Hartree" fixed point.

point" $U_{c,\mathrm{nonthermal}} < U_{c,\mathrm{thermal}}$, where the frequency of the amplitude mode vanishes. For $U_f < U_{c,\mathrm{nonthermal}}$ the time-evolution is characterized by two exponentials, a slow exponential "dephasing" followed by a faster exponential thermalization. If we plot the inverse dephasing time as a function of U_f, we again find a diverging behavior proportional to $|U_f - U_{c,\mathrm{nonthermal}}|$. The dynamics of the system in the trapped state is similar to the solution in the Hartree approximation, so that at intermediate times the system may be considered as evolving in the vicinity of a nonthermal "Hartree" fixed point (right hand panel of Fig. 6).[22] The life-time of the trapped state is finite and strongly depends on the initial value of the interaction (the larger U_i, the shorter the life-time).

Trapping phenomena of a different origin are found after quenches to large U. The left panel of Fig. 7 shows the magnetization for quenches from $U_i = 4$, $T = 0.1$ to $U_f = 6$, 7 and 8, with arrows indicating the expected values after thermalization.[23] After the quench to $U = 8$, the system will thermalize in the paramagnetic phase, but the magnetization does not immediately decay to zero. It remains trapped at a remarkably large value, and also the

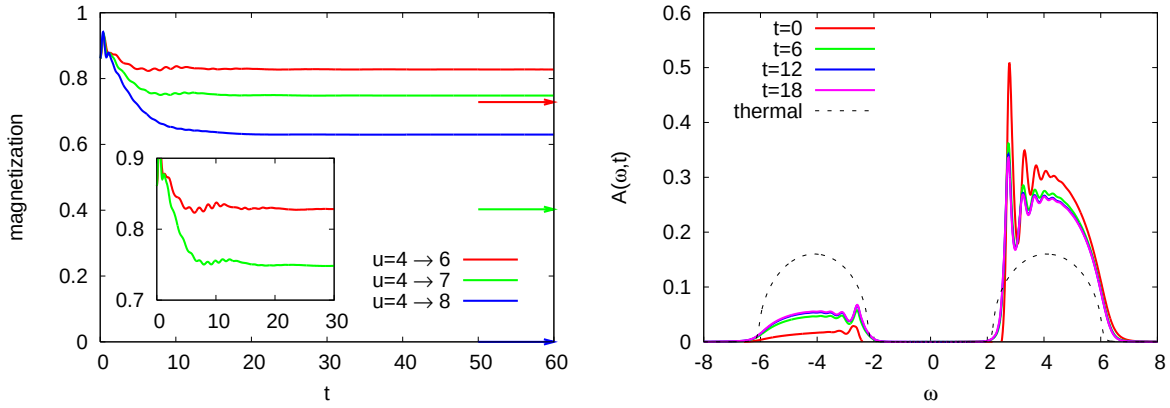

FIG. 7: Quench out of the antiferromagnetic phase in the strong-coupling regime. Left panel: Time evolution of the magnetization after quenches from $U_i = 4$ to $U_f = 6, 7, 8$. For $U_f = 8$, the system will thermalize in the paramagnetic phase, but is trapped for a long time in a transient state with a large magnetization. Right panel: Time evolution of the total spectral function for the minority spin. (From Ref. 23.)

time-resolved spectral function in the trapped state, shown in the right hand panel, shows the features (e. g. spin-polaron peaks) of an antiferromagnetically ordered system. The state after an interaction quench to $U = 8$ is similar to a photo-doped state, because double occupancies which existed as quantum-fluctuations in the initial state are "frozen" by the quench and become long-lived doublons. The trapping of the magnetization in the large-interaction regime may thus be linked to the exponentially long life-time ($\sim Ae^{\alpha(U/2)\log(U/2)}$) of artificially created doublons in a Mott insulator with large gap. If the density of frozen-in (or "photo-doped") carriers is larger than some critical value, the trapping disappears, and the magnetization relaxes to zero exponentially, with a relaxation time which depends like a power law on the distance from the trapped phase.[23]

Acknowledgments

The material presented in these notes is based on research done in collaboration with Naoto Tsuji, Martin Eckstein, Marcus Kollar, Takashi Oka and Hideo Aoki and most of the nonequilibrium DMFT discussion has been borrowed from our review article, Ref. 5.

[1] C. Giannetti, F. Cilento, S. D. Conte, G. Coslovich, G. Ferrini, H. Molegraaf, M. Raichle, R. Liang, H. Eisaki, M. Greven, et al., Nature Commun. **2**, 353 (2011).

[2] D. Fausti, R. I. Tobey, N. Dean, S. Kaiser, A. Dienst, M. C. Hoffmann, S. Pyon, T. Takayama, H. Takagi, and A. Cavalleri, Science **331**, 189 (2011).

[3] L. Stojchevska, I. Vaskivskyi, T. Mertelj, P. Kusar, D. Svetin, S. Brazovskii, and D. Mihailovic, Science **344**, 177 (2014).

[4] J. K. Freericks, V. M. Turkowski, and V. Zlatić, Phys. Rev. Lett. **97**, 266408 (2006).

[5] H. Aoki, N. Tsuji, M. Eckstein, M. Kollar, T. Oka, and P. Werner, Rev. Mod. Phys. **86**, 779 (2014).

[6] A. Georges, G. Kotliar, W. Krauth, and M. J. Rozenberg, Rev. Mod. Phys. **68**, 13 (1996).

[7] W. Metzner and D. Vollhardt, Phys. Rev. Lett. **62**, 324 (1989).

[8] M. H. Hettler, A. N. Tahvildar-Zadeh, M. Jarrell, T. Pruschke, and H. R. Krishnamurthy, Phys. Rev. B **58**, R7475 (1998).

[9] A. I. Lichtenstein and M. I. Katsnelson, Phys. Rev. B **62**, R9283 (2000).

[10] R. Peierls, Z. Physik **80**, 763 (1933).

[11] A. A. Abrikosov, L. P. Gorkov, and I. E. Dzyaloshinski, *Methods of Quantum Field Theory in Statistical Physics* (Dover, New York, 1975).

[12] G. D. Mahan, *Many-Particle Physics* (Plenum, New York, 2000), 3rd ed.

[13] L. Hedin and J. Lee, J. of Elec. Spec. and Rel. Phen. **124**, 289 (2002).

[14] J. K. Freericks, H. R. Krishnamurthy, and T. Pruschke, Phys. Rev. Lett. **102**, 136401 (2009).

[15] M. Eckstein and M. Kollar, Phys. Rev. B **78**, 245113 (2008).

[16] N. Tsuji, T. Oka, P. Werner, and H. Aoki, Phys. Rev. Lett. **106**, 236401 (2011).

[17] M. Holthaus, Phys. Rev. Lett. **69**, 351 (1992).

[18] M. Keller, W. Metzner, and U. Schollwöck, Phys. Rev. Lett. **86**, 4612 (2001).

[19] H. Shiba, Prog. Theor. Phys. **48**, 2171 (1972).

[20] A. Koga and P. Werner, Phys. Rev. A **84**, 023638 (2011).

[21] N. Tsuji, M. Eckstein, and P. Werner, Phys. Rev. Lett. **110**, 136404 (2013).

[22] J. Berges, S. Borsányi, and C. Wetterich, Phys. Rev. Lett. **93**, 142002 (2004).

[23] P. Werner, N. Tsuji, and M. Eckstein, Phys. Rev. B **86**, 205101 (2012).